N. A. Fleck,[1] *P. M. Jelf,*[1] *and P. T. Curtis*[2]

Compressive Failure of Laminated and Woven Composites

Authorized Reprint from Journal of Composities Technology & Research July 1995

REFERENCE: Fleck, N. A., Jelf, P. M., and Curtis, P. T., "**Compressive Failure of Laminated and Woven Composites,**" *Journal of Composites Technology & Research,* JCTRER, Vol. 17, No. 3, July 1995, pp. 212–220.

ABSTRACT: The effect of fiber architecture upon the compressive failure mechanisms is investigated for a wide range of fiber composites. Compressive tests are performed on both notched and unnotched specimens made from T800 carbon fiber–924C epoxy laminates, AS4 carbon fiber–PEEK laminates, 2D woven T800 carbon fiber–924 epoxy, and 3D woven AS4 carbon fiber–LY564 epoxy. Additionally, unnotched and notched compressive tests are performed on beechwood and birch plywood. In all cases, the dominant failure mechanism is by fiber microbuckling. An infinite band kinking model is used to estimate the unnotched strength and a large-scale crack bridging analysis is used to predict the notched strength.

KEYWORDS: compressive failure, composites, fracture mechanics, cohesive zone model, microbuckling

The compressive strength of composites is frequently a design-limiting parameter for long fiber, polymer matrix composites; this is partly due to the fact that the compressive strength is less than the tensile strength. In contrast, the compressive strength of monolithic solids equals or exceeds their tensile strength (by up to an order of magnitude for ceramics).

In this paper, compressive tests are reported for both unnotched specimens and specimens containing a single central hole made from the following materials: carbon fiber-epoxy laminate, two-dimensional (2-D) woven composite, 3-D woven composite, and carbon fiber-PEEK laminate. In all cases we found that the dominant failure mode is *fiber microbuckling* of the main load-bearing plies. Existing theoretical models of unnotched compressive strength [*1,2*] and of notched strength [*3*] are compared with the observed strengths and found to be adequate.

Compressive tests are also reported for unidirectional beechwood and birch plywood. It is widely recognized that woods may be regarded as fiber composites. Multidirectional wood laminates (plywood) have traditionally been used in applications requiring high specific strength. It is of practical importance to determine the extent to which the compete with modern man-made composites on the basis of specific compressive strength.

The outline of the paper is as follows. First, the crack bridging model suggested by Soutis et al. [*3*] is summarized for the prediction of the notched compressive strength of multidirectional laminates. Then, the manufacturing route and microstructure are given for each of the chosen test materials. Unnotched and notched compressive properties are reported. Finally, the crack bridging model is compared with the observed notch strengths.

[1]University reader and research associate, respectively, Cambridge University Engineering Department, Trumpington Street, Cambridge, CB2 1PZ, England.

[2]Chief, Structural Materials Center, Defense Research Agency, Farnborough, GU14 6TD, England.

Notched Compressive Strength Model of Soutis et al. [3]

Soutis et al. [*3*] have developed a crack bridging model for the initiation and growth of compressive damage from the edge of a blunt notch such as a hole. The damage zone is simulated by a compressive Mode I crack with a cohesive zone ahead of its tip. Consider compressive failure of a finite width, multidirectional composite panel, that contains a central circular hole. It is assumed that microbuckling initiates when the local compressive stress parallel to the 0° fibers at the hole edge equals the unnotched strength of the laminate σ_{un}, that is

$$k_t \sigma^\infty = \sigma_{un} \tag{1}$$

where k_t is the stress concentration factor and σ^∞ is the remote axial stress.

Damage development by microbuckling of the 0° plies, delamination, and plastic deformation in the off-axis plies is represented by a crack with a cohesive zone at its tip (Fig. 1). A linearly softening spring law is taken for the cohesive zone: the crack bridging normal traction T is assumed to decrease linearly with increasing crack face overlap $2v$ from a maximum value (equal to the unnotched compressive strength σ_{un} of the composite) to zero at a critical crack face overlap of $2v_c$. The cohesive zone is assumed to remove any singularity from the crack tip and stresses remain bounded everywhere. It is assumed that the length l of the equivalent crack represents the length of the microbuckle. When the remote load is increased the equivalent crack grows in length, thus representing microbuckle growth. The evolution of microbuckling is determined by requiring that the total stress intensity factor at the tip of the equivalent crack K_{tot} equals zero

$$K_{tot} = K^\infty + K_T = 0 \tag{2}$$

where K^∞ is the stress intensity factor due to the remote stress σ^∞ and K_T is the stress intensity factor due to the local bridging traction T across the faces of the equivalent crack. When this condition is satisfied, stresses remain finite everywhere.

The equivalent crack length l from the circular hole is deduced as a function of remote stress σ^∞ using the following algorithm. For an assumed length of equivalent crack l, we solve for σ^∞ and for the crack bridging tractions by matching the crack opening

profile from the crack bridging law to the crack profile deduced from the elastic solution for a cracked body. The cracked body is subjected to a remote stress σ^∞ and crack face tractions T. At a critical length of equivalent crack, l_{cr}, the remote stress σ^∞ attains a maximum value, σ_n, and catastrophic failure occurs.

The model contains two parameters that are measured independently from specimens made from the *same material and same lay-up:* the unnotched strength σ_{un} and the area G_c under the assumed linear traction-crack displacement curve. σ_{un} is measured from a compression test on the unnotched multidirectional laminate, and G_c is measured from a compressive fracture toughness test. The concept of compressive fracture toughness may be explained as follows. Consider a finite specimen containing a single crack, with a cohesive zone at the crack tip. The cohesive zone is assumed to be much smaller than other in-plane dimensions. Then, stresses decay remotely with radius r from the crack tip as $r^{-1/2}$, characterized by the remote Mode I stress intensity factor K. A cohesive zone exists at the crack tip such that the total stress intensity factor at the tip of the cohesive zone vanishes. Rice [*4*] has shown that the work done to advance the crack by unit area G_c equals the area under the crack traction versus crack opening displacement curve

$$G_c = 2\int_0^{v_c} \sigma(v)dv = \sigma_{un}v_c, \tag{3}$$

where $2v_c$ is the critical crack closing displacement on the crack traction-crack displacement curve, as shown in Fig. 1. For an orthotropic plate in plane stress, the fracture energy G_c is related to K_c by [*5*]

$$G_c = \frac{1}{\sqrt{2E_{xx}E_{yy}}}\left[\sqrt{\frac{E_{xx}}{E_{yy}}} + \frac{E_{xx}}{2G_{xy}} - \nu_{xy}\right]^{1/2} K_c^2 \tag{4}$$

where E and G are the laminate in-plane extensional and shear moduli, respectively, and ν is Poisson's ratio in the reference system shown in Fig. 1. This is analogous to the fracture mechanics relationship for an isotropic elastic plate in plane stress, $G_c = K_c^2/E$.

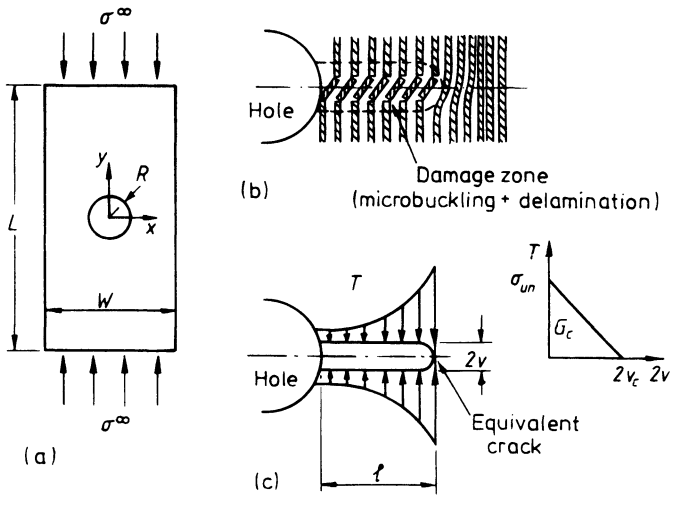

FIG. 1—*Microbuckled zone at a hole and the equivalent crack used to model the damage zone.* (a) *Schematic of compression-loaded specimen with a hole;* (b) *Microbuckled zone; damage zone (microbuckling and delamination);* (c) *Equivalent crack; a linear relation is assumed between the normal traction* T *and the crack overlap* v. G_c *is the critical value of energy release rate, and equals the area under the* T-2v *curve.*

We assume that the toughness G_c represents the total energy dissipated by fiber microbuckling, matrix plasticity in the off-axis plies, and delamination. The compressive toughness G_c of a laminate may be measured by performing a compressive fracture toughness test to measure K_c and then by using Eq 4. The compressive fracture toughness concept is meaningful provided the damage zone at the onset of crack advance is much smaller than other specimen dimensions. Also, the crack faces must not interfere at distances remote from the crack tip.

The approach has been applied to a wide range of specimen geometries [*6*] and has been used to examine the effect of lay-up upon notched strength of carbon-fiber laminates [*7*]. In the following sections, the predictions of the model discussed in Ref *3* are compared with notch-strength data for a wide range of fiber architectures.

Materials

Compressive tests were performed on both unnotched and notched specimens made from the following materials: (1) laminated T800 carbon fiber-924C epoxy, (2) laminated AS4 carbon fiber-PEEK thermoplastic, (3) 2-D woven T800 carbon fiber-924 epoxy, (4) 3-D woven AS4 carbon fiber-LY564 epoxy, (5) beechwood, and (6) birch plywood. A summary of the manufacturing route, microstructure, and mechanical properties for each material is given below.

Carbon Fiber Laminates

Laminated plates of lay-up $[(\pm 45, 0_2)_3]_s$ and an overall thickness of 3 mm were made from prepreg material of Toray T800 fibers in a Ciba-Geigy 924C epoxy matrix and AS4 carbon fibers in a PEEK matrix [*8,9*]. The AS4 carbon fibers are less strong and stiff than Toray 800 fibers and PEEK is tougher than 924C epoxy.

Woven Laminates

The 2-D laminate consists of 12 plies of (0°/90°) woven prepreg; it was made from Toray T800 carbon fibers in a Ciba-Geigy Fibredux 924 epoxy matrix and was laid up at the Farnborough Defence Research Agency. Each prepreg sheet contains axially aligned warp tows ('stuffers') interwoven with transverse weft tows ('fillers') as a 5-harness satin-weave conventional textile, as sketched in Fig. 2*a*. A typical section of the composite is given in Fig. 2*b;* the section plane contains both the axial and the through-thickness directions. The degree of misalignment of the axial warp tows is clearly visible.

The 3-D composite (supplied by Cambridge Consultants Limited) is of the through-the-thickness angle interlock type and comprises BASF Celion G30-500 carbon fibers in a matrix of Ciba-Geigy LY564 araldite combined with the hardener HY2954. The microstructure consists of five layers of straight, axial warp tows (stuffers) of 3 by 12 k dernier with a center-center spacing of 6.35 mm (Fig. 3*a*). Weft tows of 12 k dernier are aligned in the transverse direction, and warp-weaver tows of 6 k dernier (0.4-mm thick) run on an inclined plane through the thickness of the composite from one face to the other. The wavelength of the warp-weaver tows at the surface of the plate is 5.35 mm. Figure 3*b* shows a polished section of 3-D laminate in which warp-weaver tows are clearly visible.

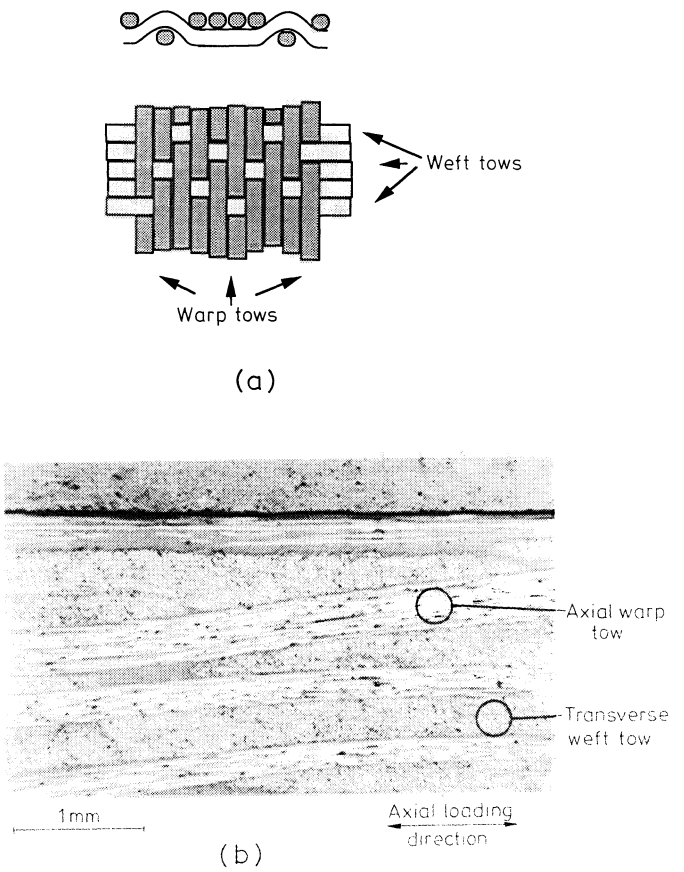

FIG. 2—*The fiber architecture of 2-D (0°/90°) woven composite, made from Toray T800 carbon fibers in a Ciba-Geigy Fibredux 924 epoxy matrix.* (a) *sketch of architecture and* (b) *axial section showing waviness of axial warp tows.*

The fiber volume fractions of the various tows in the 2-D and 3-D composites were estimated by optical observation of axial and transverse sections. Fiber volume fractions for the constituent elements of both the 2-D and 3-D woven composites are given in Table 1. The volume fraction of fibers in the axially aligned warp tows V_{fa} has a dominant influence on the axial properties of the 2-D and 3-D woven composites. For the 2-D composite $V_{fa} \approx 0.3$, whereas for the more complicated 3-D structure, $V_{fa} \approx 0.25$. These estimates are consistent with the measured values of axial modulus for the composites, as summarized in Table 2 by the following argument. A crude rule of mixtures estimate for the axial modulus E gives $E \approx V_{fa}E_f$ where E_f is the axial modulus of the fibers. For

TABLE 1—*Volume fractions of fiber orientations in 2-D and 3-D woven composites.*

Volume Fraction	2-Dimensional Weave	3-Dimensional Weave
Axial warp fibers	0.3	0.25
Transverse weft fibers	0.3	0.25
Warp-weaver fibers	...	0.05

TABLE 2—*Measured properties of the composites under investigation.*

Material	Axial Modulus, GPa	Unnotched Compressive Strength, σ_{un}, MPa	Compressive Fracture Toughness, K_c, MPa$\sqrt{m}$	$\equiv \frac{1}{\pi} K_c^2/\sigma_{un}^2$, mm
$[(\pm 45/0_2)_3]_s$ T800–924C	88.0	810	46.5	1.05
$[(\pm 45/0_2)_3]_s$ AS4–PEEK	72.8	720	52.8	1.71
$[(0°/90°)_3]_s$ 2D-woven T800–924C	65.3	335	59.7	10.1
3D-woven G30–500 fibers in LY564 matrix	60.1	356	33.5	2.82
0° beechwood	13.7	66.7	8.71	5.43
(0/90/0/90/0) birch plywood	10.0	45.7	5.31	4.30

the 2D weave, E_f = 248 GPa and the estimated axial modulus E = 74.4 GPa is in good agreement with the measured value of 65.3 GPa. For the 3D weave, E_f = 234 GPa and the estimated axial modulus E = 58.5 GPa is, again, in good agreement with the measured value of 60.1 GPa.

Optical microscopy was used to examine the degree of waviness in the load bearing warp tows of each woven system. The 3-D system was designed to display a high degree of axial alignment with very little sinusoidal waviness of the warp tows, as shown in Fig. 3*b*. Maximum deviation of these tows from the axial direction is only 1 to 2°. In the 2-D laminate warp tow waviness is more significant with maximum angles of deviation of 4 to 5° (Fig. 2*b*).

Woods

Microstructure of Wood—Wood exists as a fiber composite on the microscopic scale [*10,11*]. In general, the 'fibers' (visible to the eye as the grain of the wood) can be regarded as hollow tubes. Typically,

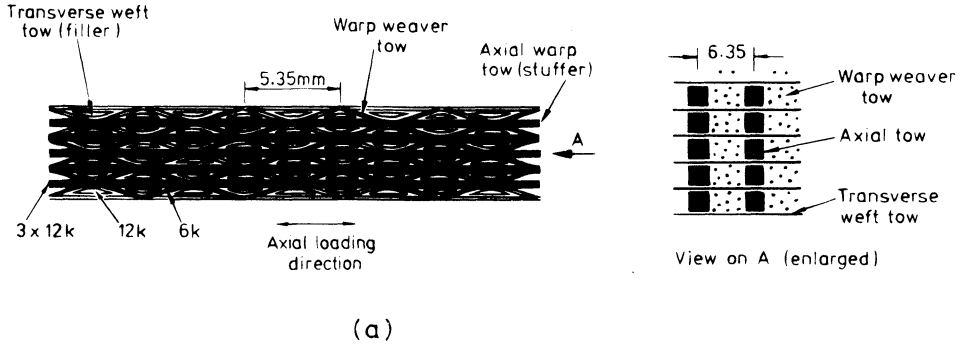

FIG. 3*a*—*The fiber architecture of 3-D woven composites, made from BASF Celion G30-500 carbon fibers in a matrix of Ciba-Geigy LY564 Araldite. Sketch of fiber architecture.*

the cell wall is composed of four layers: the outer or primary wall P and three inner or secondary walls S_1, S_2, S_3 (Fig. 4). These layers are in turn composed of an arrangement of microfibrils. It is the microfibrils to which the role of fiber is assigned. The microfibrils are surrounded by a matrix of hemicellulose and lignin (an aromatic compound amorphous in structure); this long fiber composite makes up each cell wall layer. It is expected that the orientation of microfibrils plays a significant role in determining the cell's axial properties. Typically, the middle S_2 layer comprises over 75% of the entire cell-wall thickness and the microfibrils are aligned at an angle of 10 to 30° to the axis of the cell.

Unnotched and notched compressive tests were performed on beechwood and on birch plywood. The 5-mm thick beech test pieces were machined so that the long axis of the specimens coincided with the grain orientation. The birch plywood was constructed from 5 plies, each 1-mm thick; the two outer plies and the central-ply were oriented with the grain parallel to the axial load bearing direction. The grain direction of the two remaining plies was aligned transversely to this axial direction.

Mechanical Testing

Tests were performed to measure unnotched compressive strength, notched compressive strength, and compressive fracture toughness. The basic specimen geometry is shown in Fig. 5*a* for all materials considered [*12*]. The exception is the specimen geometry for the unnotched compressive strength of the unidirectional beechwood and 5-ply birch; specimens of width $w = 8$ mm and thickness $t = 5$ mm were tested using a Celanese test rig [*13*]. In the Celanese rig, the compressive load is applied to the specimen by shear transfer from the fixture wedges; end tabs on the specimens are not required.

The scale of the specimen geometry was chosen in order for the test to be representative of material response, particularly for the woven composites where the fiber tow diameter is of the order of 1 mm. Tests were performed on a screw driven test machine operating at a cross-head speed of 0.017 mm s^{-1}. Euler macrobuckling of the specimens was inhibited by a PTFE-lined antibuckling guide [*13*] (Fig. 5*b*). The antibuckling guide has a central window of dimension 90-mm long by 38-mm wide, and the bolts were made finger-tight. The specimens were loaded in shear by means of wedge grips.

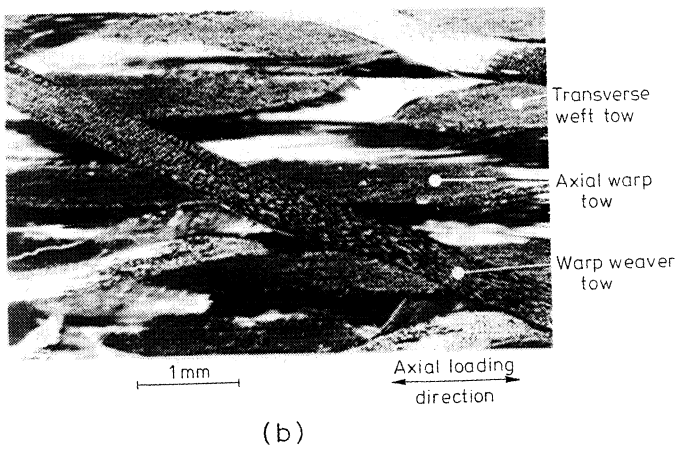

FIG. 3*b*—*The fiber architecture of 3-D woven composites, made from BASF Celion G30-500 carbon fibers in a matrix of Ciba-Geigy LY564 Araldite. Axial section showing through-thickness warp-weaver tows.*

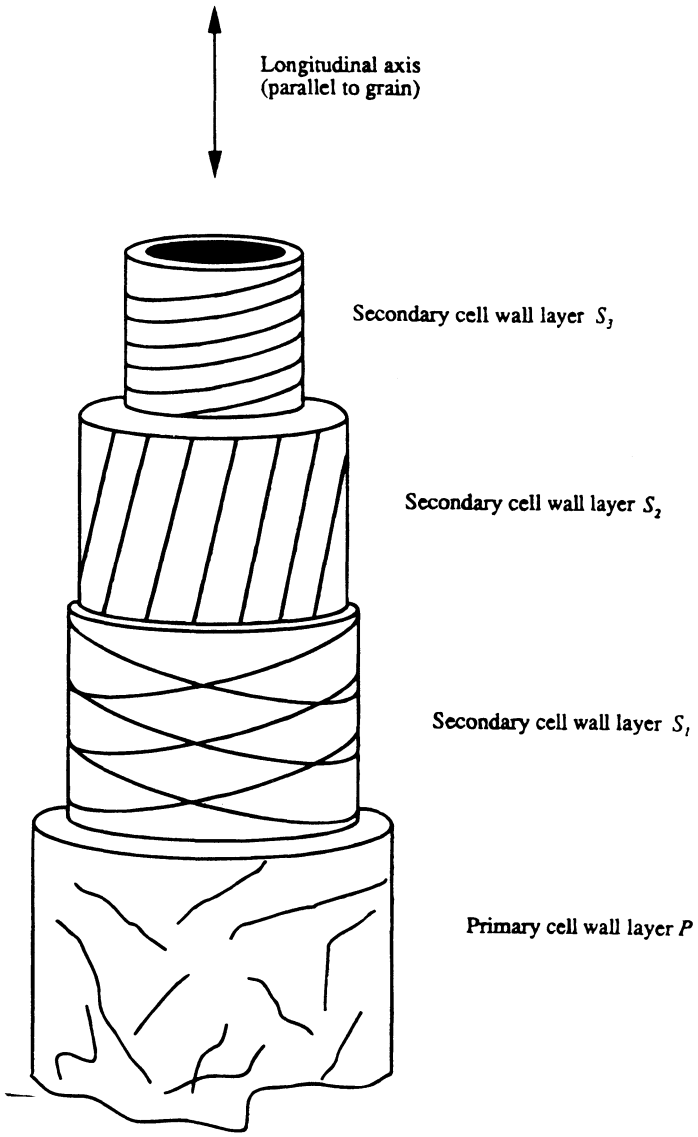

FIG. 4—*Sketch of typical cell wall for wood.*

The strain response of unnotched specimens was measured using thin-foil strain gages bonded to both faces of the test-piece. Bending effects were then measured, and suitable alignment of the grips was performed to reduce bending effects to a negligible level (less than 5% difference between front and back face strain). Relatively large-scale gages (5 by 2 mm) were used to avoid local strain concentrations caused by tow-size effects. The load and strain were recorded at regular intervals throughout each test by a computer-controlled data logger. Compressive fracture toughness test pieces contained central razor-sharpened slits of length 10 to 20 mm; the specimens behaved in an elastic-brittle manner and the compressive fracture toughness K_c was measured from the failure load. Finite element calculations by the authors confirmed that the K calibration for the center cracked panel is almost identical to that for an isotropic plate, and is given in standard textbooks (for example, Paris and Sih [5]; Tada et al. [*14*]. Notched specimens contained a single central hole of diameter $d = 5$ to 25 mm. Typically, three valid experimental results were averaged to give the values reported below. However, only one to two notched tests were performed on the woven composites due to the limited availability of test material.

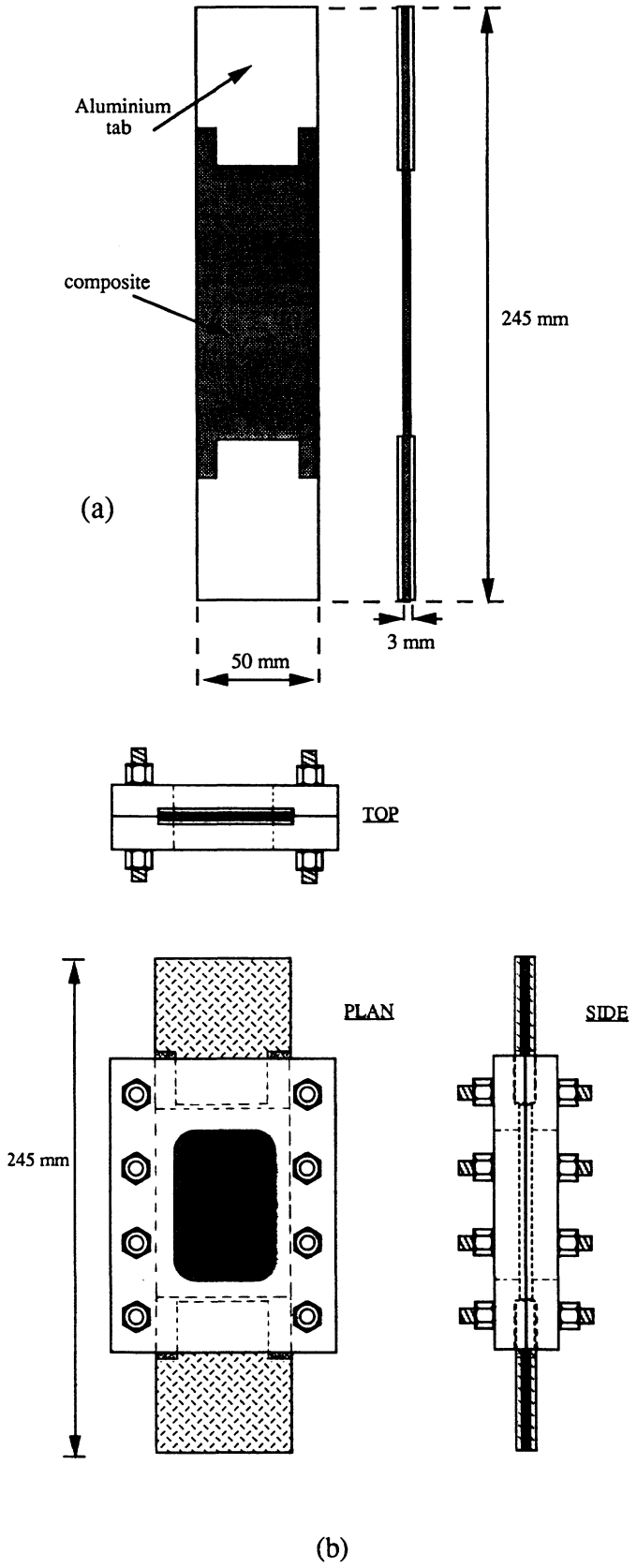

FIG. 5—(a) *Test specimen geometry and* (b) *antibuckling guide to restrain macrobuckling.*

Results for Unnotched Strength

Laminated Composites

The compressive stress-strain response is almost linear to failure for the $[(\pm 45,O_2)_3]_s$ laminates of T800-924C and AS4-PEEK. The failure strain for both laminates is 1.0 to 1.2%. The slightly higher failure stress of 810 MPa for the T800-924C material, compared with 720 MPa for AS4-PEEK, reflects the higher modulus of the T800 carbon fibers compared to the AS4 fibers. Soutis et al. [7] have already discussed the effect of laminate lay-up upon unnotched failure strain; they found that the failure strain is almost insensitive to the orientation of lay-up. This is supported by the current results where we observe that failure is controlled by microbuckling of the 0° plies (Fig. 6*a*).

2-D and 3-D Woven Composites

For both the 2-D and 3-D woven composites, the compressive stress-strain response is almost linear to fracture. The axial elastic modulus of the 2-D system is slightly higher than that of the 3D system; this observation is consistent with the fact that the 2-D weave has a higher volume fraction of axially aligned fibers than the 3-D weave. Compressive fracture of the unnotched woven specimens is dominated by plastic microbuckling of the load-bearing axial stuffers. Figures 6*b* and 6*c* show polished optical micrographs of axial sections of both materials taken after compressive failure. Characteristic microbuckled bands are evident in the axial tows.

The transverse weft tows of both woven materials suffer matrix failure on a plane at approximately 45° to the axial loading direction. The warp-weaver tows of the 3-D woven composite also fail by plastic microbuckling, as shown in Fig. 6*d*.

The compressive strength of $\sigma_c = 356$ MPa for the 3-D material is higher than that for the 2-D laminate ($\sigma_c = 335$ MPa). These compressive strength data may be used to infer the degree of fiber misalignment in the 2-D and 3-D woven materials. Assume that at the instant when compressive failure occurs, the matrix in the off-axis tows is at yield while the axially aligned warp tows support the stress necessary to trigger plastic microbuckling. The strength of the warp tows can then be deduced from the rule-of-mixtures expression

$$\sigma_c = \sigma_f V_{fA} + \sigma_{my}(1 - V_{fA}) \tag{5}$$

where σ_c is the compressive strength of the composite, V_{fA} is the volume fraction of axial tows, σ_f is the stress supported by the axial tows, and σ_{my} is the matrix compressive yield strength. The deduced value of axial tow compressive strength σ_f is substituted into Argon's expression for compressive strength due to plastic microbuckling [1]

$$\sigma_f = k/\bar{\phi} \tag{6}$$

where $\bar{\phi}$ is the initial average fiber misalignment angle and k is the matrix shear yield strength. For the 2-D weave, we assume $k = 60$ MPa and $\sigma_{my} = 110$ MPa, and for the 3-D weave we assume $k = 40$ MPa and $\sigma_{my} = 70$ MPa. By combining Eqs 5 and 6, the unnotched compressive strength data are used to infer a fiber misalignment angle of $\bar{\phi} = 1.9°$ for the 3-D weave and $\bar{\phi} = 4.1°$ for the 2-D system. As discussed above, observation of polished axial sections of the woven composites show that the warp tows

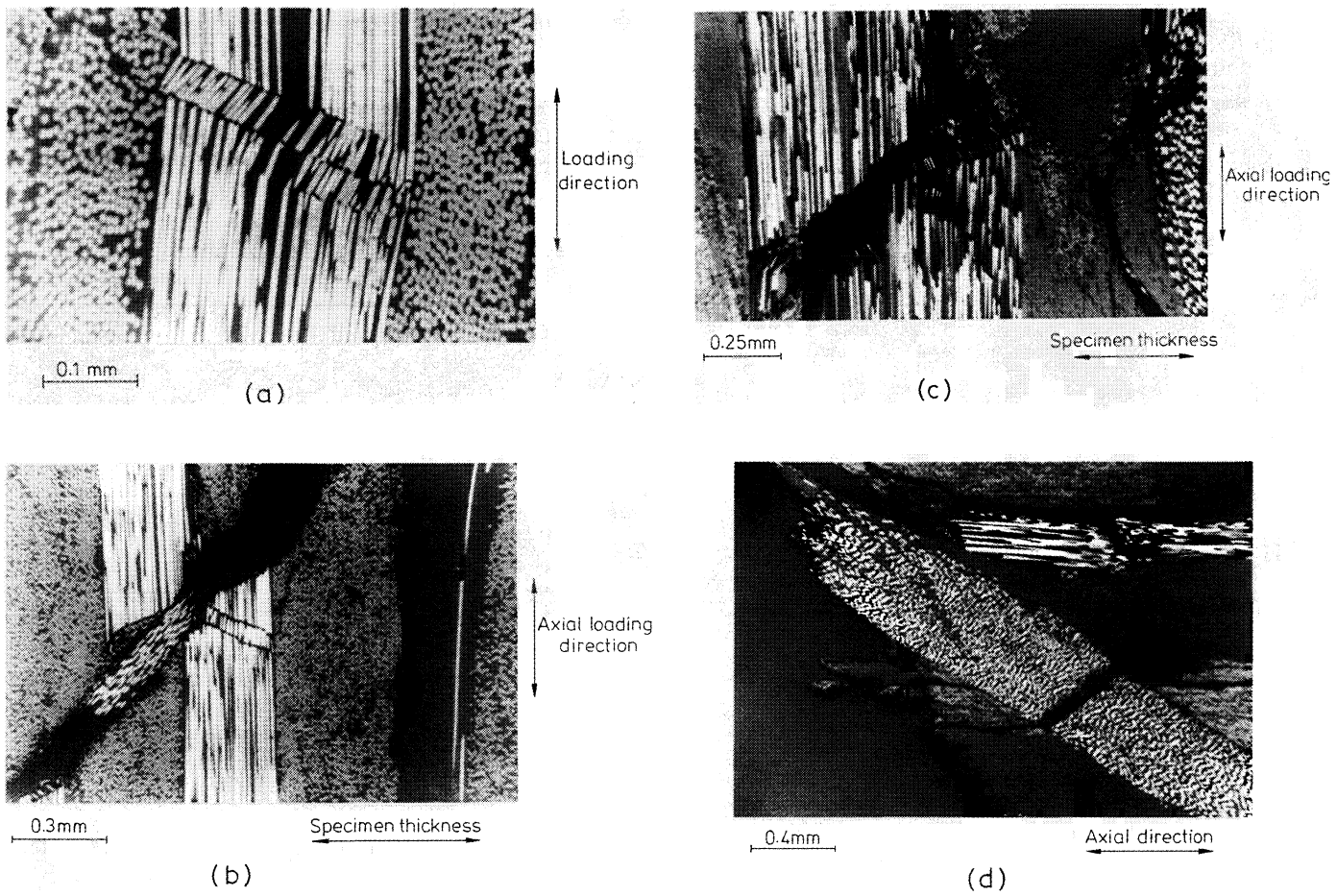

FIG. 6—(a) *Multidirectional AS4-PEEK laminate immediately prior to maximum load. The figure shows an optical micrograph of a polished section normal to the specimen width direction;* (b) *Optical micrograph of unnotched 2-D woven composite after failure. Microbuckling of the 0° plies is evident. The large lateral slip is a consequence of the sectioning and mounting process;* (c) *Optical micrograph of unnotched 3-D woven composite after failure; note the microbuckling of the 0° plies;* (d) *Scanning electron micrograph showing microbuckling of the warp weaver tow in the 3-D woven composite.*

have a maximum misalignment angle of 1 to 2° for the 3-D weave and 4 to 5° for the 2-D weave. Thus, the inferred fiber misalignment angle $\bar{\phi}$ is in good agreement with the physically observed waviness of axial tows for both systems.

Optical microscopy further shows that in both woven systems there is a distribution of fiber misalignment of 2 to 3° *within* the axial warp tows similar to that observed in unidirectional fiber composite material. Further experimental and theoretical work are required to clarify the role of fiber waviness *distribution* upon compressive strength.

Woods

The unnotched compressive strengths of the beech wood and the 5-ply birch wood are given in Table 2. We note that the compressive strengths are about an order of magnitude less than those of the carbon fiber-epoxy laminates. Since the density of the beech and birch woods is about 1/3 that of the carbon fiber laminates, the *specific compressive strength* (*unnotched strength/density*) of the woods is about 1/3 that of the carbon fiber laminates. We shall show that the underlying reason for the relatively low specific strength of the woods is the large degree of fiber misalignment in the load bearing S_2 layer of the cell walls of the wood.

In order to investigate the mechanism of compressive failure in woods, a compressive test was performed on a sample of Norwegian spruce *in-situ* in the scanning electron microscope (SEM). This species of wood was chosen because it possesses a highly regular cellular structure with few knots. Specimen dimensions (width w = 3.5 mm, thickness t = 3.5 mm, length L = 5 mm) were chosen so as to avoid Euler buckling. In order to reveal the wood microstructure, a thin sliver of wood was removed from the surface with a new sharp razor blade immediately prior to testing.

The encircled regions in Fig. 7 show damage in the primary P wall, caused by internal microbuckling of the S_2 cell-wall layer of a spruce specimen. The photograph was taken at a load of approximately 60% of the failure load. At higher levels of applied load multiple plastic microbuckles combine to produce a concertina-like collapse of the axial cell walls (Gibson and Ashby [*11*]). The microbuckling theory of Argon [*1*] is used to estimate the fiber misalignment angle in the S_2 layer. The microbuckling strength σ_f of the S_2 cell-wall material is given by Eq 6, where k is the shear yield strength of the cell-wall material. The axial cell-wall stress can be inferred from the average remote stress σ^∞ by assuming that the S_2 cell-wall material, of volume fraction V_f, carries the whole of the axial load. Then

$$\sigma^\infty = \sigma_f V_c \tag{7}$$

Similarly, the remote shear load is assumed to be carried by the

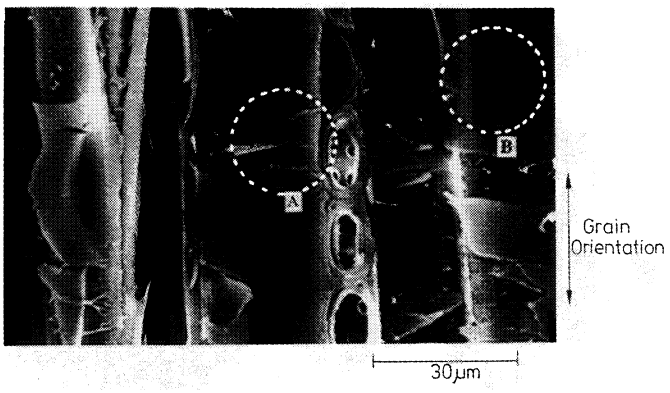

FIG. 7—*Scanning electron micrograph showing microbuckling of the cell walls of Norwegian spruce.*

S_2 layers; the macroscopic shear strength of the wood τ^∞ is related to the local strength of S_2 cell-wall material k by

$$\tau^\infty = kV_c \tag{8}$$

Equations 7 and 8 combine to give

$$\bar{\phi} = \frac{k}{\sigma_f} = \frac{\tau^\infty}{\sigma^\infty} \tag{9}$$

Upon substituting values quoted by Dinwoodie [*10*] for Norwegian spruce of σ^∞ = 36.5 MPa and τ^∞ = 9.8 MPa, we infer an average microfibril misalignment angle of $\bar{\phi}$ = 26°. Observations of the S_2 layer using the SEM give a measured misalignment angle for the microfibrils of 25 to 30°, in support of Argon's microbuckling theory [*1*]. Further support for the accuracy of Eq 6 has been given by Budiansky and Fleck [*2*] and by Fleck et al. [*15*]. They show that Eq 6 is in good agreement with experimental data for a wide range of unidirectional composites. Also, they show that the use of more sophisticated constitutive laws for the composite than the rigid-perfectly plastic assumption give only a small improvement in the accuracy of Eq 6, provided the value of shear yield strength k used in Eq 6 is taken from the in-plane shear stress versus shear-strain response for the composite at a value of shear strain of about 1%.

Notched Compressive Strength, Sharp Slit and Circular Hole

In this section the effect of a single hole upon the compressive strength is reported for the laminated carbon fiber composites, woven composites, and woods. The cohesive zone model suggested by Soutis et al. [*3*] is then compared with measured notched strengths. The model assumes that compressive failure is initiated by the formation of a plastic microbuckle at the edge of the notch; the microbuckle then grows in a stable manner until it reaches a critical length. At this point unstable propagation occurs and the specimen fails catastrophically. The notched strength σ_n is defined by the maximum load divided by the gross cross-sectional area. The model takes as input two independently measured material parameters: the unnotched compressive strength σ_{un} and compressive toughness G_c.

Carbon Fiber Laminates

Panels made from T800-924C and AS4-PEEK containing a central hole were loaded in compression-to-failure. The typical damage state immediately prior to failure is shown in Fig. 8*a* for an AS4-PEEK specimen. (The T800-924C failed in a qualitatively similar manner.) Microbuckles initiate from the edge of the hole in both the 0 and 45° plies; some splitting of the 0° plies and delamination between the 0° plies and the 45° plies are also apparent.

The evolution of microbuckle length with remote applied stress was monitored periodically by interrupting a test and X-raying the specimen; a typical response showing initial stable microbuckle development prior to catastrophic failure is given in Fig. 8*b*. The predicted response by the Soutis et al. model [*3*] is included in the figure and is in good agreement with the observed initiation and growth of a microbuckle. The model slightly underestimates the stress for initiation of a microbuckle but accurately predicts both the maximum load and the associated microbuckle length.

The notched strength σ_n of the T800-924C material is compared with that of the AS4-PEEK material in Fig. 8*c*. Again, predictions of the Soutis et al. theory [*3*] are included in the figure; excellent agreement is found between theory and experiment for both materials. The AS4-PEEK material has a higher fracture toughness (55 MPa$\sqrt{\text{m}}$) than the T800-924C laminate (46 MPa$\sqrt{\text{m}}$) and is less notch-sensitive. The notched strengths of both materials lie between the limits of notch insensitivity (where the net section failure stress equals the unnotched strength) and the perfectly brittle limit (where the local stress at the root of the notch equals the unnotched strength).

Woven Materials

The failure sequence of notched woven specimens was observed (1) with a traveling microscope of the side face of the specimen during compressive loading, and (2) with a scanning electron microscope of the fracture faces after completion of the test. We deduce that compressive failure of the notched 2-D and 3-D woven composites is by microbuckling of the axial warp tows from the hole. Again, the stable growth of a microbuckle under increasing remote load is superseded by the attainment of maximum load at a critical length of microbuckle. No axial splitting from the edges of the hole is observed.

The 2-D weave displays a higher compressive fracture toughness (K_C = 59.7 MPa$\sqrt{\text{m}}$) than the 3-D system (K_C = 33.5 MPa $\sqrt{\text{m}}$). The relatively high toughness of the 2-D laminate is reflected by the notched compressive strength tests. The introduction of an 8-mm central hole reduced the 3-D laminate compressive strength by 37%, whereas a larger 10-mm central hole resulted in a strength reduction of only 27% in the 2-D material.

The 2-D woven composite also possesses a significantly higher compressive fracture toughness than a conventional nonwoven laminate with identical constituents: Soutis et al. [*7*] report a value of K_C = 40.6 MPa$\sqrt{\text{m}}$ for a $[(0/90_2/0)_3]_S$ lay-up of T800-924 laminate, compared with K_C = 59.7 MPa$\sqrt{\text{m}}$ for the woven material. However, the woven composite has a lower unnotched strength of 335 MPa compared with 670 MPa for the $[(0/90_2/0)_3]_S$ laminate.

The Soutis et al. cohesive zone model [*3*] was used to predict the growth of a microbuckle and the compressive strength of both 2-D and 3-D woven composites. The input parameters to the model are the measured unnotched compressive strength σ_{un} and the compressive toughness G_c of the each composite. A comparison of the predicted and observed microbuckle growth as a function of load is given in Fig. 9*a* for the 2-D weave system; the predicted evolution of microbuckle length with increasing remote stress is in satisfactory agreement with optical measurements of microbuckle growth. The

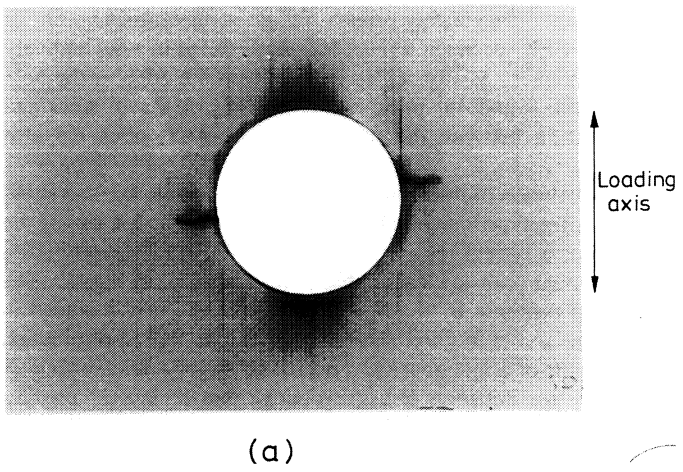

FIG. 8—(a) *Dye penetrant enhances X-ray micrograph of* $[(\pm 45,0_2)_3]_S$ *AS4-PEEK laminate, with 10-mm diameter central hole;* (b) *Comparison of the predictions of the Soutis et al. model* [3] *with the observed growth of a microbuckle from a 5-mm central hole in a* $[(\pm 45,0_2)_3]_S$ *AS4-PEEK laminate;* (c) *Comparison of the measured and predicted compressive strengths* σ_n *for* $[(\pm 45,0_2)_3]_S$ *AS4-PEEK and T800-924c laminates. The panels are of width* w = *50-mm wide, and the notch strength is plotted as a function of hole radius* R. *The theoretical predictions are given by the Soutis et al. model* [3].

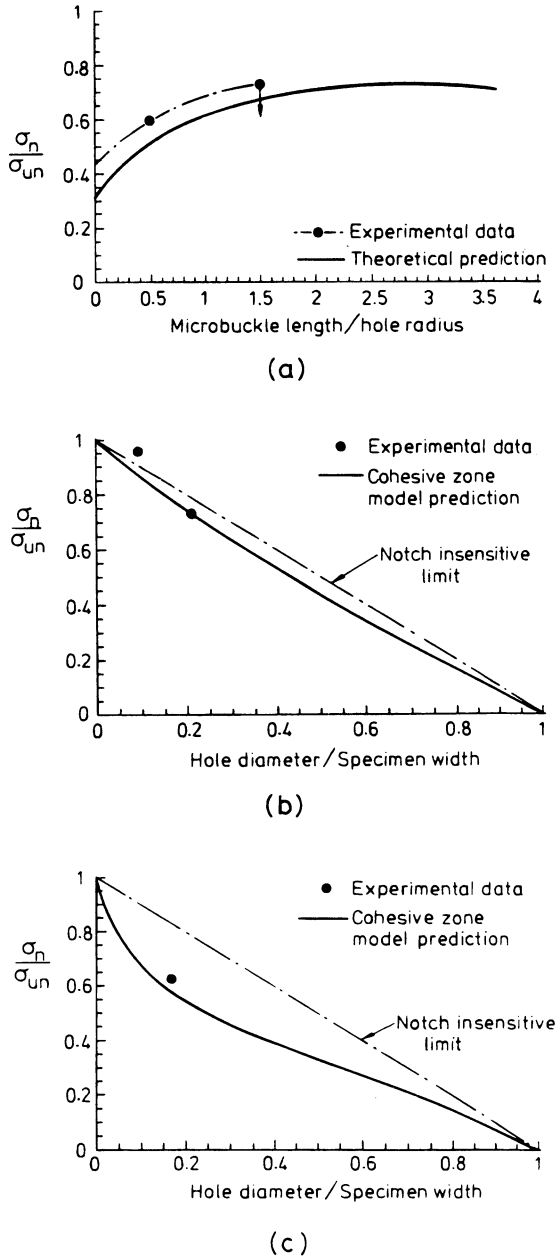

FIG. 9—(a) *Comparison of observed microbuckle growth with prediction of Soutis et al. model* [3] *for the 2-D woven composites containing a central hole of diameter 10 mm;* (b) *Comparison of measured notched strength with prediction of Soutis et al. model* [3] *for the 2-D woven composites;* (c) *Comparison of measured notched strength with prediction of Soutis et al. model* [3] *for the 3-D woven composites.*

notch strength predictions of the cohesive zone model are compared with the observed strengths in Fig. 9*b* for the 2-D weave and in Fig. 9*c* for the 3-D weave. We conclude that the notch-strength model adequately predicts the relatively notch-insensitive behavior of the 2-D system and the more notch-sensitive response of the 3-D laminate.

Woods

Failure of the notched unidirectional beech and birch plywood specimens is by the initiation and growth of a crease from the central hole. The cohesive zone model (using the material proper-

ties of unnotched compressive strength and compressive fracture toughness) accurately predicts the notched compressive strength of both the unidirectional beech and birch plywood (Figs. 10*a* and 10*b*). For both materials the experimental results and the model predictions lie close to the net section stress-failure criterion (that is, failure occurs when the stress in the ligament material surrounding the hole equals the unnotched failure strength). We conclude that unidirectional beech and birch plywood have high damage tolerance; stress raisers degrade strength only insofar as they reduce the cross-sectional area of the specimen or component.

Conclusions

Compressive failure mechanisms have been determined for a wide range of fiber architectures in carbon fiber composites and woods. The dominant failure mechanism in both unnotched and notched specimens is plastic microbuckling of the load bearing axial tows.

The cohesive zone model of Soutis et al. [*3*] is successful in predicting the notched compressive strength for a wide range of composites. The model takes as input the unnotched compressive strength σ_{un} and the compressive toughness G_c, which are independently measured for any given composite material and lay-up. The toughness G_c is related to the fracture toughness K_c by way of Eq 7 and thereby to a characteristic length scale a_t defined by

$$a_t = K_c^2 / \pi\sigma_{un}^2 \qquad (10)$$

We may interpret a_t as the size of the damage zone (microbuckle zone size) at the tip of a long crack, or as the transition flaw size at which the failure criterion switches from strength to fracture toughness. Cohesive zone models such as that given by Soutis et al. [*3*] attempt to smoothly switch from the limit of strength-governed design (where the flaw size a is much less than a_t) to the limit of fracture toughness governed (where the flaw size a is much greater than a_t). The material length scale a_t further serves as a useful measure of damage tolerance. From the tabulated values of a_t included in Table 2, we conclude that both woven composites and woods have a low compressive strength and a high damage tolerance; a major reason for the low compressive strength is the large value of fiber misalignment.

Acknowledgments

The authors are grateful to Mr. R. Edgson of Cambridge Consultants Ltd. for the provision of the 3-D woven material and to Dr. M. P. F. Sutcliffe for helpful discussions. Financial support is gratefully acknowledged from the Procurement Executive of the Ministry of Defense (Contract 2029/267) and the Office of Naval Research (Contract 0014-91-J-1916).

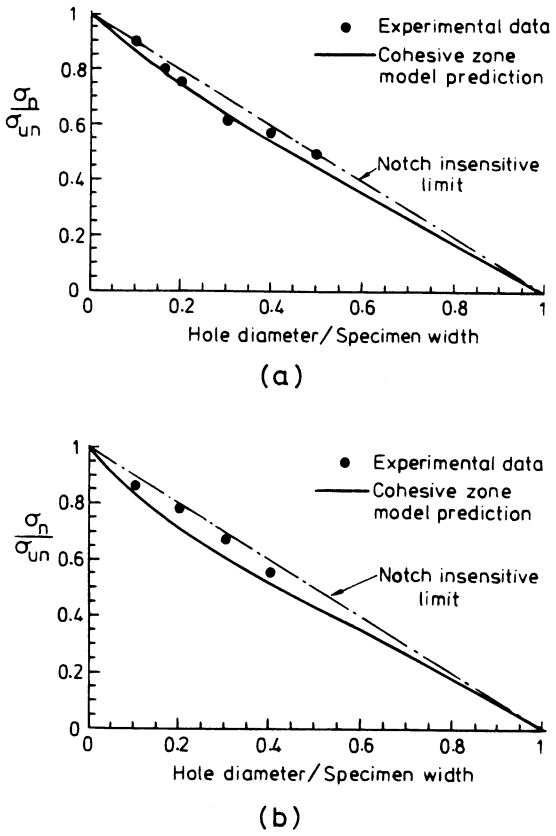

FIG. 10—*Comparison of measured notched strength with prediction of Soutis et al. model* [*3*] (a) *beech wood and* (b) *birch plywood.*

References

[*1*] Argon, A. S., "Fracture of Composites," *Treatise of Material Science and Technology,* Vol. 1, Academic Press, New York, 1972.

[*2*] Budiansky, B. and Fleck, N. A., "Compressive Failure of Fiber Composites," *Journal of the Mechanics and Physics of Solids,* Vol. 41, No. 1, 1993, pp. 183–211.

[*3*] Soutis, C., Fleck, N. A., and Smith, P. A., "Failure Prediction Technique for Compression-Loaded Carbon Fiber-Epoxy Laminate with Open Holes," *Journal of Composite Materials,* Vol. 25, No. 11, 1991, pp. 1476–1498.

[*4*] Rice, J. R., "Mathematical Analysis in the Mechanics of Fracture," Vol. 2, Chapter 3, *Fracture,* H. Leibowitz, Ed., Academic Press, New York, 1968.

[*5*] Paris, P. C. and Sih, G. C., "Stress Analysis of Cracks," *Fracture Toughness Applications, ASTM STP 381,* American Society for Testing and Materials, Philadelphia, 1969, pp. 30–83.

[*6*] Sutcliffe, M. P. F. and Fleck, N. A., "Effect of Geometry Upon Compressive Failure of Notched Composites," *International Journal of Fracture,* Vol. 59, 1993, pp. 115–132.

[*7*] Soutis, C., Fleck, N. A., and Curtis, P. T., "Compressive Failure of Notched Carbon Fibre Composites," Proceedings of Royal Society, London, Vol. 440, 1993, pp. 241–256.

[*8*] Soutis, C., "Compressive Failure of Notched Carbon Fibre-Epoxy Panels," Ph.D. Thesis, Cambridge University Engineering Dept., 1989.

[*9*] Jelf, P. M., "Compressive Failure of Aligned Fiber Composites," Ph.D. Thesis, Cambridge University Engineering Dept., 1992.

[*10*] Dinwoodie, J. M., *Timber, Its Nature and Behaviour,* Van Nostrand Reinhold Co. Ltd., Berkshire, England, 1981.

[*11*] Gibson, L. J. and Ashby, M. F., *Cellular Solids, Structures and Properties,* Pergamon Press plc, Headington Hill Hall, Oxford, OX3 OBW, England, 1988.

[*12*] Soutis, C., "Measurement of the Static Compressive Strength of Carbon-Fibre/Epoxy Laminates," *Composite Science and Technology,* Vol. 42, 1991, pp. 373–392.

[*13*] Curtis, P. T., "CRAG Test Methods for the Measurement of the Engineering Properties of Fibre Reinforced Plastics," *RAE Technical Report 85099,* 1985.

[*14*] Tada, H., Paris, P. C., and Irwin, G., "The Stress Analysis of Cracks Handbook," 2nd edition, Paris Productions, St. Louis, MO, 1985.

[*15*] Fleck, N. A., Deng, L., and Budiansky, B., "Prediction of Kink Width in Fiber Composites," to appear in *Journal of Applied Mechanics,* 1995.